Thermodynamic and Kinetic Study of the Carbothermal Reduction of SnO2 for Solar Thermochemical Fuel Generation

ARTICLE *in* ENERGY & FUELS · FEBRUARY 2014

Impact Factor: 2.79 · DOI: 10.1021/ef402182g

2 AUTHORS, INCLUDING:

Gael Leveque
École Polytechnique Fédérale de Lausanne
7 PUBLICATIONS **27** CITATIONS

energy&fuels

Article

pubs.acs.org/EF

Thermodynamic and Kinetic Study of the Carbothermal Reduction of SnO_2 for Solar Thermochemical Fuel Generation

Gaël Levêque and Stéphane Abanades*

Processes, Materials, and Solar Energy Laboratory (PROMES), French National Center for Scientific Research (CNRS), 7 Rue du Four Solaire, 66120 Font-Romeu, France

ABSTRACT: The carbothermal reduction of SnO_2 is studied as part of a two-step thermochemical process for solar fuel production. A second law analysis was applied to validate a combined methane cracking−SnO_2 carbothermal cycle, which shows 86% theoretical exergy efficiency and an energy content upgrading of 28.2%. Thermodynamics predicts a predominance of solid−solid reactions over 700 °C ($SnO_2 + C \rightarrow Sn + CO_2$, and $SnO_2 + 2C \rightarrow Sn + 2CO$), while a plausible two-step solid−gas mechanism can also be speculated ($SnO_2 + 2CO \rightarrow Sn + 2CO_2$, and $C + CO_2 \rightarrow 2CO$). Two carbon types were selected to investigate the reaction mechanism, a high specific surface area activated charcoal, and a nanosized carbon black obtained from solar methane cracking. The activated carbon favors the solid−gas mechanism (activation energy of 267 kJ mol^{-1}), while carbon black favors direct solid−solid reduction through a slower but complete reaction with a first-order reaction mechanism and a lower activation energy (204 kJ mol^{-1}), opening opportunities for improved profitability of both methane cracking and redox cycles for solar fuel generation.

1. INTRODUCTION

Fossil fuel depletion and the environmental impact of their generalized use on the climate stability are major issues for the upcoming century. New sustainable and carbon-free energy sources are of paramount interest. Solar energy is a clean and widespread renewable energy source because it is available at any place where human life is present but in a diluted and intermittent state. Concentrating solar technologies allow for a dense form of this energy, typically available at higher temperature than could be with any nuclear power plant (above 1000 °C). Solar concentrated energy can be either converted into conventional power energy using thermodynamic cycles or used to produce solar fuels (in the form of hydrogen, syngas, and synthetic hydrocarbon fuels),[1,2] e.g., via decarbonization of a carbonaceous feedstock (fossil hydrocarbons or biomass)[3,4] or via thermochemical H_2O and CO_2 splitting cycles.[1,5] On the one hand, decarbonization of a fossil fuel is well-represented by natural gas cracking, described by the following reaction:

$$CH_4 \rightarrow C + 2H_2 \qquad \Delta G^\circ = 0 \text{ kJ/mol at } 547\ ^\circ\text{C} \qquad (1)$$

The methane molecule is split into hydrogen and carbon black that can be stored or valorized because this material exhibits many commercial applications (such as polymer reinforcement used in the tire industry),[6] and hydrogen can be used as a carbon-free fuel. The reaction can proceed either thermally at a high temperature (typically above 1400 °C) or with a catalyst at a lower temperature (typically in the range of 900−1200 °C).[3] The use of solar energy aims to substitute the use of fossil fuels for supplying the process energy, and the main benefits are thus fossil fuel savings and reduction of CO_2 emissions compared to conventional processes. The Solhycarb EU project (FP6) has been one of the most advanced projects for non-catalytic solar methane splitting,[7,8] during which a pilot-scale solar reactor has been developed and carbon black has been produced and characterized.[9] Its quality highly depends upon experimental conditions, so that part of the production may not be valuable as a high-value industrial product (transient production). Because the economical viability of methane cracking is highly linked to the carbon black selling price,[6] other potential uses for this unmarketable co-product are of great interest.

On the other hand, solar-driven thermochemical cycles[10−12] have the potential to convert water and carbon dioxide into H_2 and CO as high-value solar fuels with high energy content. The harvesting of solar energy through thermochemical cycles is generally composed of two steps when based on metal oxide redox pairs (Figure 1a). The cycled metal oxide species is first thermally reduced at a high temperature, yielding oxygen and the reduced lower valence metal oxide. Then, the latter is reoxidized in the presence of water and/or carbon dioxide to produce hydrogen and/or carbon monoxide that can be directly burnt for power/heat generation to release the harvested energy or turned into dense liquid fuels through Fischer−Tropsch conversion. Alternatively, carbothermal processes can also be considered to decrease the temperature of the endothermal reduction step using a reducing carbonaceous reagent (e.g., C or CH_4).[13] The major difference with thermal reduction is the use of a carbonaceous agent to promote the reduction at a lower temperature, yielding CO (Figure 1b) that can be either processed as formed (syngas production) or transformed into more H_2 via water−gas shift (WGS) reaction. Note that, when using biomass sources, such as wood charcoal (biochar) or biogas, the net global contribution of CO_2 to the atmosphere is zero and the system is fully benign from an ecological point of view. The coupling of the carbothermal process with methane cracking as a source of solid carbon was

Received: November 4, 2013
Revised: December 17, 2013

   dx.doi.org/10.1021/ef402182g | Energy Fuels XXXX, XXX, XXX−XXX

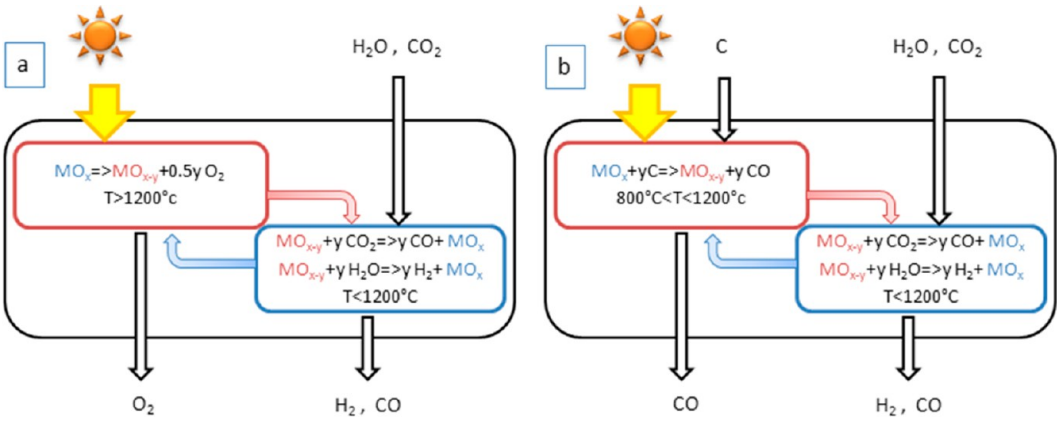

Figure 1. Metal oxide redox cycles: (a) thermal cycle and (b) carbothermal cycle.

theoretically investigated, and its interest was proven via a second law analysis.[14] Recently, carbothermal ZnO reduction has been tested in an unprecedented packed-bed pilot-scale reactor.[15,16] Energy conversion efficiency (ratio of heating values of products to the thermal energy input) of 30% was obtained in a 300 kW pilot plant.[15] These first operationnal tests conducted in the range of 1000−1200 °C highlighted some important features: most of the thermal losses are due to re-radiation at the aperture of the thermochemical reactor as a result of the high-temperature conditions, and Zn particle collection is required. New carbothermal systems can be proposed to improve the process, with SnO_2/Sn being one of the most promising.

solar carbothermal reduction (endothermic)

$$SnO_2 + 2C \rightarrow Sn + 2CO$$
$$\Delta G^\circ = 0 \text{ kJ mol}^{-1} \text{ at } 641\ ^\circ\text{C} \quad (2)$$

syngas production/re-oxidation (exothermic)

$$Sn + \alpha CO_2 + (2-\alpha)H_2O \rightarrow SnO_2 + \alpha CO + (2-\alpha)H_2, \quad 0 < \alpha < 2 \quad (3)$$

Epstein et al.[17] have listed the main advantages of the latter over the ZnO/Zn system: (1) The oxide reducing temperature is lower by 200−300 °C (850−900 °C for the SnO_2/Sn system versus 1100−1200 °C for the ZnO/Zn system). A lower temperature reduces re-radiation losses, thus resulting in a higher thermal efficiency, and alleviates material requirement for the reactor. (2) Zinc is produced in the gaseous phase, which means that the quenching of the off-gases is mandatory to avoid the back reaction as well as the separation of suspended solid Zn particles from the off-gas stream. This step is inefficient on both material and thermal viewpoints. Nanodust is not easy to collect, and sensible heat can hardly be recovered. In contrast, metallic tin is produced in solid or liquid phase, so that it can be easily handled, while gaseous products can be cooled in a conventional heat exchanger.

In contrast, the shortcomings associated with the tin-based carbothermal cycle relate to higher prize and lower abundance of Sn compared to Zn, lower fuel production, sensitivity of the fuel production rate to reduced tin morphology, and possible presence of residual carbon in reduced tin powder.

Of utmost importance is the first step consisting of SnO_2 carbothermal reduction, because of the high temperature involved. The first study on the subject[18] aimed to produce metallic tin from finely ground stannic oxide ore (cassiterite) and carbon. Apart from classical parameters, such as temperature, particle size, and reactant composition, the influence of the type of carbon was studied (graphite or coconut charcoal). The speculated mechanism is based on two steps: $SnO_2 + 2CO \rightarrow Sn + 2CO_2$, and $CO_2 + C \rightarrow 2CO$. Thus, the reaction mechanism does not involve solid−solid reactions but rather two solid−gas reactions, with the latter (also known as the Boudouard reaction) being the limiting step, which explains the presence of CO_2 in the gas products. SnO formation was not observed during the reaction, and CO_2 was predominantly produced. The authors report that charcoal particle size does not seem to have an impact on the reduction rate: because the charcoal particles used are porous, reducing the particle size does not significantly improve its specific surface area.[18] Increasing the temperature favors the reaction, whereas increasing the carbon content has a negative effect, because the limiting phenomenon becomes the gas diffusion into solids. The type of carbon has a significant effect: the reduction starts at 800 °C with an activation energy of 220.9 kJ/mol when using coconut charcoal, while the reduction with graphite starts at 925 °C with an activation energy of 323.8 kJ/mol. This difference may be attributed to the presence of minerals in the coconut charcoal that have a catalytic effect. The study also points out the catalytic behavior of the metallic tin for the carbon oxidation reaction, recently confirmed by Epstein et al.,[17] although a two-stage cyclic mechanism (namely, Sn oxidation to SnO_2 with CO_2 in excess, followed by SnO_2 carboreduction until complete carbon consumption) may also be anticipated. The latter have reported an activation energy of the carbothermal reduction of 235.4 kJ/mol for a similar temperature with beech charcoal as the carbon source.

A theoretical study was conducted to evaluate the most promising thermochemical reaction of the (SnO_2/SnO/Sn) + (C/CH_4) systems based on thermodynamic consideration, efficiency calculation, and evaluation of the energy benefit.[19] It was shown that the carbothermal reduction of SnO_2 features a higher solar-upgrading potential compared to the methanothermal reduction reaction, and it may be thus an efficient way of harvesting solar power. The use of solid carbon may also be preferred to the use of a gaseous reducing agent (methane for example) because of the difficulties arising from gas separation (reducing agent CH_4/produced CO).

Besides, the second step of the process that consists of the hydrolysis of tin has been experimentally demonstrated in a controllable reaction.[17,20] Thus, an experimental investigation

dx.doi.org/10.1021/ef402182g | Energy Fuels XXXX, XXX, XXX−XXX

Table 1. Second Law Analysis and Comparison of Two Carbothermal Cycles, ZnO/C and SnO_2/C[a]

	methane cracking	+combined with the ZnO/C cycle	+combined with the SnO_2/C cycle
Q_{solar} (kW) = $\Delta H_{reduction}/\eta_{reactor}$	181	461	234
$Q_{reactor,net}$ (kW) = $\Delta H_{reduction}$	171	434	227
Q_{quench} (kW) = $\int_{T_{reduction}}^{T_{ambiant}} C_p\, dT$	−96	−194	−48.3
W_{FC} (kW) = $\Delta G_{3H_2+CO+2O_2=3H_2O(l)+CO_2 \text{ at } 25\ ^\circ C}$	−474 (for $2H_2 + O_2$)	−969	−969
Q_{FC} (kW) = $\Delta H_{3H_2+CO+2O_2=3H_2O(l)+CO_2} - W_{FC}$	−98 (for $2H_2 + O_2$)	−171	−171
η_{exergy} (%) = $\frac{W_{FC}}{\sum Q_{solar} + HHV_{CH_4}}$	29.4	71.6	86.0
fuel upgrading (%) = $\frac{\sum_i n_i HHV_i}{HHV_{CH_4}}$	8.5	28.2	28.2

[a] p = 1 bar. DNI: I = 1 kW m^{-2}. Concentration ratio: C = 5000. Results normalized to $\dot{n}_{CH_4}$ = 1 mol s^{-1}. $\eta_{reactor}$ = absorption efficiency of the reactor assuming a perfectly insulated black body cavity receiver. Thermodynamic properties from HSC Outokumpu code.[21]

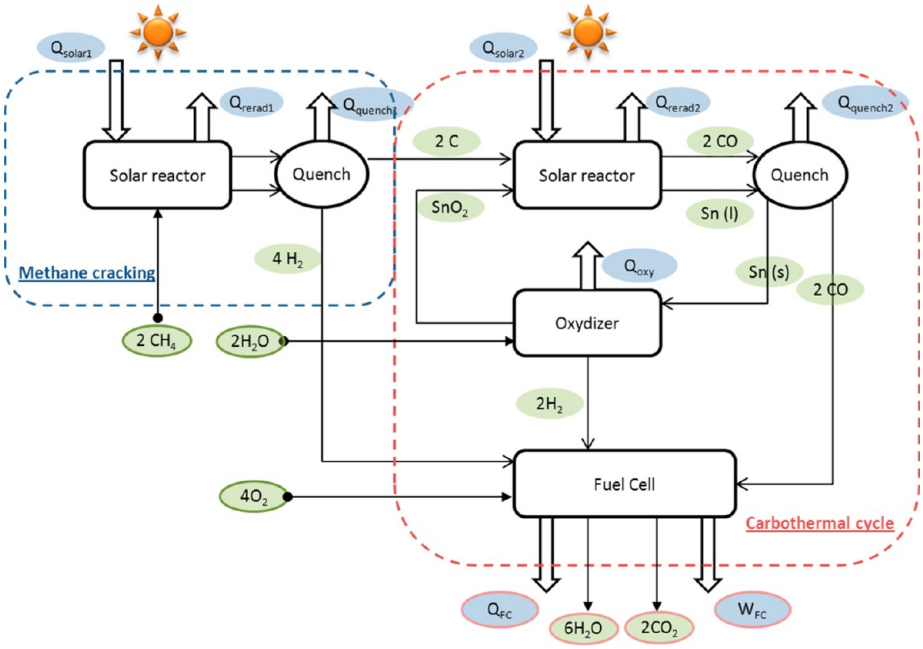

Figure 2. Flow sheet diagram of the proposed combined methane cracking/SnO_2 carbothermal cycle process.

of the SnO_2/Sn solar carbothermal cycle seems pertinent, also studying the option to use solar-produced carbon black as a reducing agent.

2. THERMODYNAMIC ANALYSIS

2.1. Global Process Analysis. To assess the potential of the combined methane cracking/SnO_2 carbothermal cycle process, the second law analysis for ZnO carboreduction[14] is compared to the corresponding one for the tin cycle. Results are summarized in Table 1, and the flow diagram is presented in Figure 2 for SnO_2. Both methane cracking and ZnO carbothermal reduction are considered at 1200 °C, whereas SnO_2 carbothermal reduction is assumed to occur at 1000 °C. In the fuel upgrading expression, "i" stands for the energy-containing products: C and H_2 for methane cracking (n_C = 1, and n_{H_2} = 2) and H_2 and CO for the combined methane cracking/carbothermal cycles (n_{H_2} = 3, and n_{CO} = 1). The most important difference between the two carbothermal cycles is the fact that only half a SnO_2 mole is reduced per mole of carbon, highly decreasing the needed solar power. Another important feature relates to the quenching of the products of ZnO/C reduction necessary to stop the reverse reaction, which results in 4 times more energy lost than that for the SnO_2/C cycle. The exergy efficiency is improved with the SnO_2/C cycle because the same amount of energy is produced through syngas, while the needed solar power is lessened.

2.2. Carbothermal Reduction Thermochemistry. To understand and predict the mechanisms taking part in the SnO_2 carboreduction, the Gibbs free enthalpy of the possible reactions is plotted as a function of the temperature (Figure 3). For clarity's sake, reactions involving SnO were not represented because previous works[17,18] tend to prove its absence or at least its minor participation.

$$SnO_2 + 2C \rightarrow Sn(s, l) + 2CO \quad (4)$$

$$SnO_2 + C \rightarrow Sn(s, l) + CO \quad (5)$$

$$SnO_2 + 2CO \rightarrow Sn(s, l) + 2CO_2 \quad (6)$$

$$CO_2 + C \rightarrow 2CO \quad (7)$$

According to thermodynamics, only CO is capable of reducing SnO_2 below 600 °C. At 700 °C, reactions 4−6 have similar Gibbs free

dx.doi.org/10.1021/ef402182g | Energy Fuels XXXX, XXX, XXX−XXX

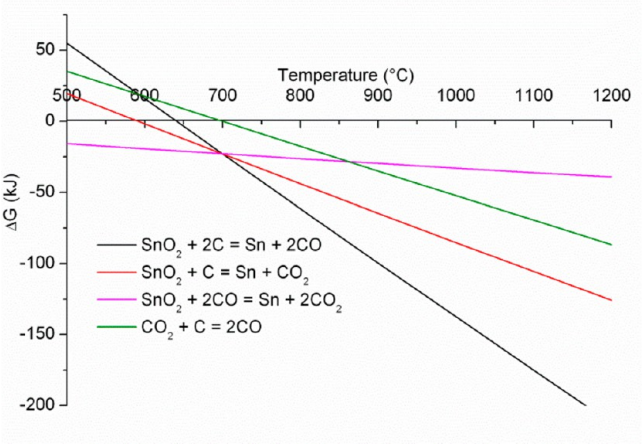

Figure 3. Gibbs free enthalpy variation associated with possible reactions during SnO_2 carbothermal reduction.

enthalpy and Boudouard reaction 7 starts. As the temperature rises, reaction 4 is the most favored reaction, followed by reaction 5. At about 850 °C, a shift appears between reactions 6 and 7, with the Boudouard reaction being preponderant. Thus, the carbothermal reduction follows multiple and simultaneous paths. The thermodynamically most favored reactions over 700 °C are represented by reactions 4 and 5. As the temperature rises, the CO_2 produced by the previous path tends to turn back into CO via Boudouard reaction 7 and to reduce SnO_2 via reaction 6.

This description of the involved phenomena does not corroborate the previously reported experimental observations,[18] where reactions 6 and 7 are preponderant. This can be explained by the fact that the most thermodynamically favored reactions 4 and 5 are solid−solid reactions. Thus, the actual reaction rate may be highly impacted by interface phenomena and oxygen ion diffusion limitations in solid bulk, and solid/gas reactions may predominate.

Figure 4 summarizes the equilibrium composition of a SnO_2 + 2C mixture as a function of the temperature computed with HSC

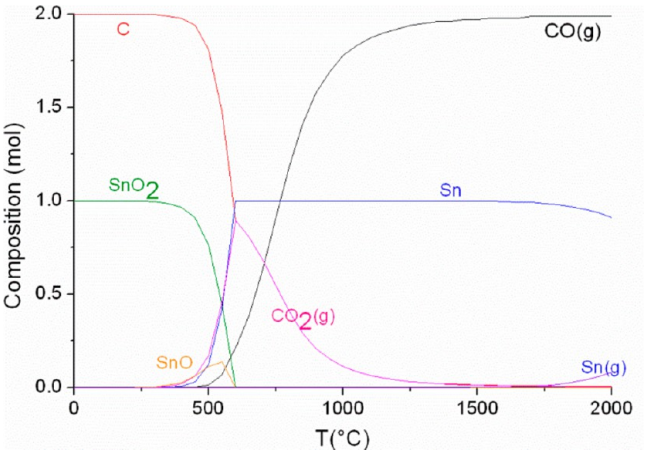

Figure 4. Equilibrium composition of the SnO_2 + 2C system at 1 bar without inert gas dilution.

Chemistry software.[21] The reaction starts significantly at about 500 °C with SnO as a reaction byproduct. At 600 °C, SnO_2 is fully converted to liquid Sn with CO_2 as the main gaseous product, following reaction 5. Above 750 °C, CO is the prevailing product. At 1000 °C, more than 85% of carbon is converted into CO and SnO_2 is reduced to metallic tin at thermodynamic equilibrium. This is the reference temperature chosen for next calculations. At this temperature, the effect of the composition of the solid reactant mixture is studied (Figure 5). At 1000 °C in thermodynamic equilibrium, SnO_2 is fully reduced with

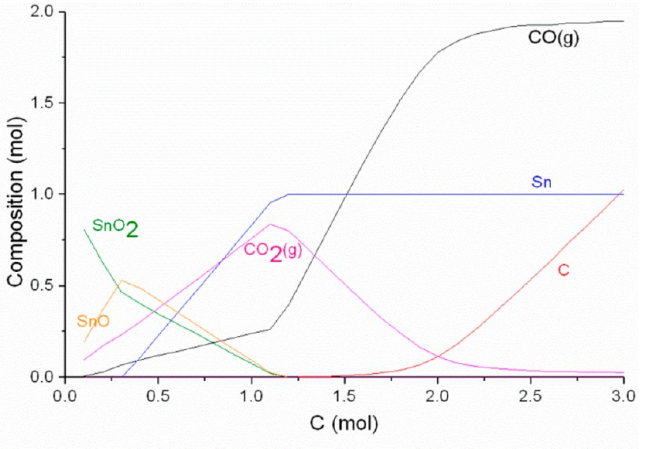

Figure 5. Equilibrium composition at 1000 °C as a function of the carbon content in the reactant mixture (1 mol of SnO_2; P = 1 bar; no dilution).

1.25 mol of carbon and CO_2 is the main species produced. To reach higher CO production, an excess of carbon must be used but at the expense of more carbon that remains in the solid phase, which may lead to diffusion limitations.[18] The clarification of the reaction pathway is among the scope of the experimental section of this study.

3. EXPERIMENTAL STUDY OF SNO_2 CARBOTHERMAL REDUCTION

3.1. Experimental Setup and Methods. The objective of the experimental study is to investigate the kinetics of the carbothermal reduction reaction and to estimate the effect of the carbon type [activated charcoal, ash content of 3.5%, steam activation, Sigma Aldrich Darco (AC in the following) or carbon black produced from thermal methane cracking (CB in the following)], composition of the reactant (carbon/oxide mole ratio), and heating rate. Table 2 summarizes the main

Table 2. Physical Properties of the Reactant Powders

	size (μm)	specific surface area (m^2/g)	micropore area (m^2/g)	external surface area (m^2/g)
activated charcoal Darco	<149	732	426	306
carbon black	<33 × 10^{-3}	44		44
SnO_2 (Merck, 99%)	<5	7		7

properties of the reactant powders as the result of Brunauer−Emmett−Teller (BET) characterization via N_2 adsorption/desorption at 77 K (Micromeritics Tristar 3020). A more thorough characterization of the CB can be found in ref 9. Amorphous carbons, such as AC and CB, generally show the highest reactivity compared to highly ordered carbons with reduced active sites. From Table 2 arise major differences between carbon types, with CB being composed of particles much smaller than SnO_2 particles (2 orders of magnitude for the biggest particles) with medium surface area, while AC is composed of particles bigger than SnO_2 particles (2 orders of magnitude) with much higher specific surface area and micropore area that should favor solid−gas reactions. Not mentioned is the apparent density, twice as high for AC as for CB. While AC is expected to promote the Boudouard reaction through its high specific surface area, thus, the mechanisms

dx.doi.org/10.1021/ef402182g | Energy Fuels XXXX, XXX, XXX−XXX

Table 3. Description of the Realized Experimental Runs

run	heat ramp (K/min)	reactant	sample mass (g)/composition (mol_C/mol_{SnO_2})	apparatus
1	10	SnO_2 + 3AC	0.5772/2.99	tube flow reactor
2	5	SnO_2 + 3AC	0.5790/2.99	tube flow reactor
3	10	SnO_2 + 2AC	0.5401/2.09	tube flow reactor
3 bis	10	SnO_2 + 2AC	0.5963/2.09	tube flow reactor
4	5	SnO_2 + 2AC	0.5438/2.09	tube flow reactor
5	10	SnO_2 + 3CB	0.6017/3.00	tube flow reactor
5 bis	10	SnO_2 + 3CB	0.3317/3.00	tube flow reactor
6	5	SnO_2 + 3CB	0.4938/3.00	tube flow reactor
7	10	SnO_2 + 2CB	0.5615/2.08	tube flow reactor
8	5	SnO_2 + 2CB	0.5777/2.08	tube flow reactor
9	8	SnO_2 + 2AC	0.5297/2.09	tube flow reactor
10	10	SnO_2 + AC	0.5773/1.16	tube flow reactor
11	15	SnO_2 + 3CB	0.0437/3.00	TGA
12	10	SnO_2 + 3CB	0.0443/3.00	TGA
13	10	SnO_2 + 3AC	0.0716/2.99	TGA

reported in previous studies,[17,18] CB is expected to promote both solid−solid reactions thanks to a favored particle contact and the Boudouard reaction.

Two different complementary apparatuses were used for kinetic analysis of the carbothermal reduction: (1) a thermogravimetric analyzer (TGA, Setaram Setsys Evolution) equipped with a mass spectrometer for gas species identification and (2) a tube flow reactor (50 mm inner diameter alumina tube, with a heated length of 180 mm) consisting of a horizontal electrically heated tube furnace equipped with a CO−CO_2 online analyzer using a non-dispersive infrared sensor (MGA3000; full scale, 0−100% CO_2 and 0−30% CO; repeatability, ±1% full scale). The tube flow reactor was used to quantify precisely the composition of the gas released during sample heating. A given weight of SnO_2/carbon reactant (about 0.5 g placed at the center of the heated tube in an alumina crucible, with a sample height of 2−3 mm) was subjected to heat ramps with linear heating rates of 5−10 K min^{-1} in a stream of argon (0.2 N L min^{-1}), and the outlet gas was analyzed continuously. In contrast, the experiments using the TGA were performed for reaction progress quantification based on the variation of the sample weight during thermal treatment while qualitatively identifying the gas species released during the reaction by mass spectrometry. During heating, the residual absorbed volatile species were removed below 200 °C, so that they could not interfere with the reaction. Table 3 summarizes the experimental runs and operating conditions, and reproducibility tests were successfully achieved for both AC and CB.

3.2. Results and Discussion. *3.2.1. Thermogravimetric Analysis.* Non-isothermal runs were conducted with a linear heating rate of 10 or 15 K min^{-1} up to 1200 °C under neutral atmosphere (Ar = 40 N mL min^{-1}), for sample mass of about 44 mg for CB and 72 mg for AC. With the densities of the involved carbons being different, the same volume of reactant in the crucible was used. Figure 6 shows the influence of the heating rate and carbon type on the reaction rate. The reaction starts earlier with AC (about 750 °C), and the mass loss follows a two-sloped linear trend. The first half of the curve is parallel to the corresponding curve relative to CB. The heating rate has little effect because the weight loss curves relative to CB are parallel for 10 and 15 K min^{-1}.

Results of TGA runs with coupled mass spectrometry for CO and CO_2 are shown in Figures 7 and 8 for SnO_2 + 3AC and SnO_2 + 3CB, respectively. Note that the amounts of gas species detected at low temperatures are due to the presence of residual air (residual CO_2 in air and N_2 with the same atomic mass as CO are detected). For AC, the reaction rates are higher than for CB, and the shift in the time course of CO and CO_2

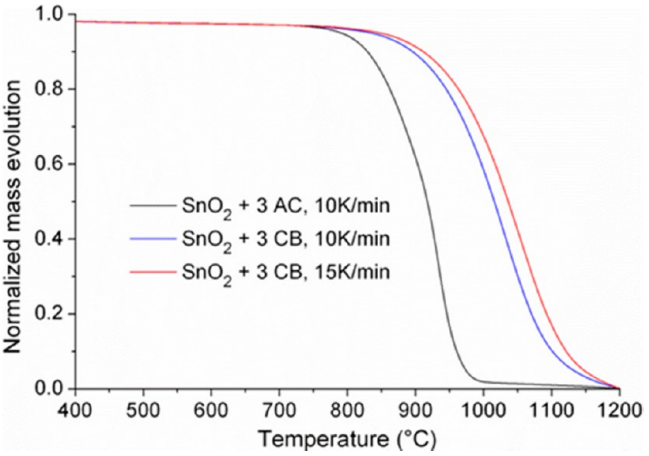

Figure 6. Normalized mass evolution $((m_{final} - m(t))/(m_{final} - m_{initial}))$ as a function of the temperature during SnO_2 carbothermal reduction.

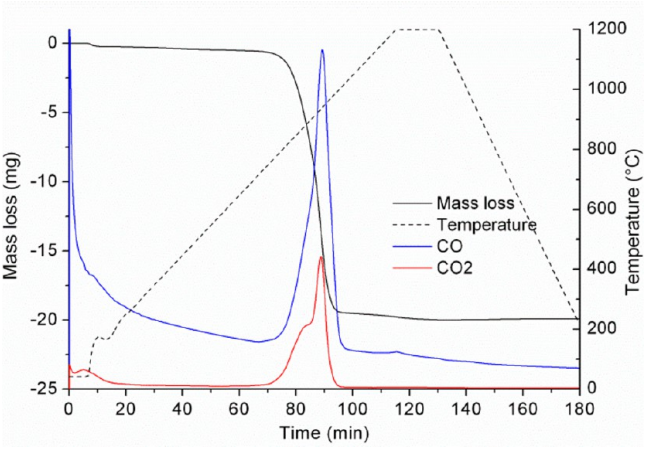

Figure 7. Temporal evolution of the mass loss and relative CO/CO_2 concentration profiles obtained from TGA (SnO_2 + 3AC; 10 K/min).

dx.doi.org/10.1021/ef402182g | Energy Fuels XXXX, XXX, XXX−XXX

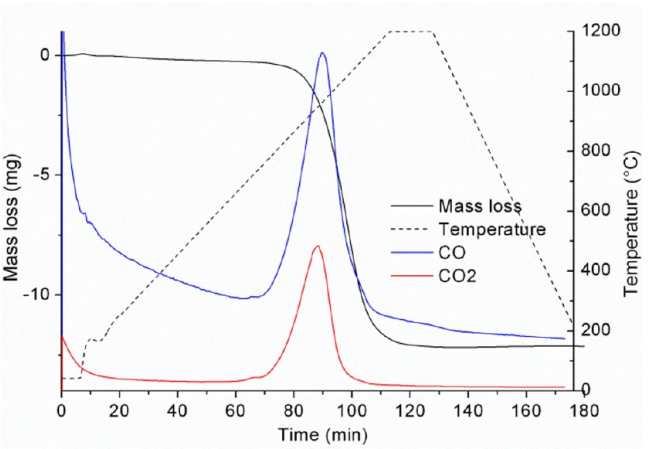

Figure 8. Temporal evolution of the mass loss and relative CO/CO_2 concentration profiles obtained from TGA (SnO_2 + 3CB; 10 K/min).

evolution suggests two different mechanisms. The normalized concentration versus temperature profiles (Figure 9) emphasize

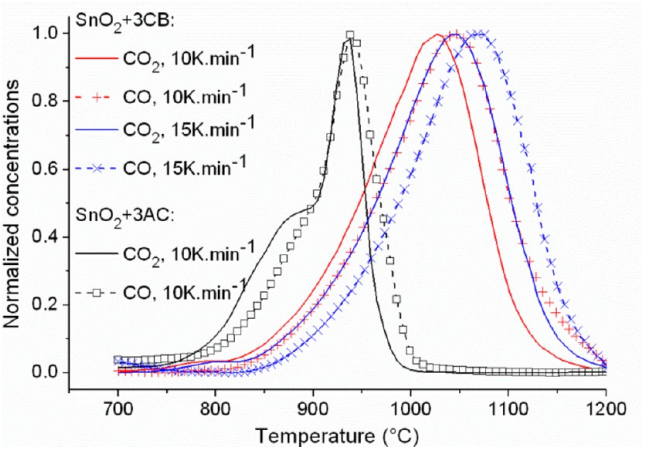

Figure 9. Normalized CO and CO_2 concentrations as a function of the temperature for the two carbon sources obtained from TGA.

clearly these statements. The peak reaction rate is reached at 925 °C for AC versus 1050 °C for CB. The inflection point in the CO_2 evolution for AC is observed from 875 to 900 °C, which corresponds to an instantaneous increase in the production of CO and a sharpening of the mass loss evolution (as observed in Figure 7), and this behavior is attributed to the start of the Boudouard reaction consuming CO_2. This can be explained from the shift between Gibbs free enthalpy of reactions 6 and 7 observed in Figure 3: consumption of CO_2 by the Boudouard reaction becomes higher than its generation through SnO_2 reduction by CO. Then, a new equilibrium settles between the two gas/solid reactions, leading to a higher reduction rate. Thus, the Boudouard reaction seems to be favored in the SnO_2 + 3AC system. On the other hand, gas species evolution during carbothermal reduction with CB follows a more constant yet not so sharp slope, pointing out a more uniform mechanism.

3.2.2. Tube Flow Reactor. The carbothermal reduction was then investigated in a tube flow reactor with continuous outlet gas analysis for CO/CO_2 concentration measurement during the progress of the reaction. Because previous studies report a negative effect of an excess of carbon on the reaction linked to diffusion limitations,[18] a comparison was made between the instantaneous production rate of CO (normalized to the maximum potential production, $\dot{n}_{CO}/2n_{SnO_2,initial}$) of the different experiments as a function of the temperature. CO temporal evolution was chosen as a marker of the evolution of the reaction because it is the main product and detected with more accuracy than CO_2 by the online analyzer. The amount of CO_2 released in the different experiments was then obtained from a global mass balance and corresponds to the difference between the sample mass variation and the amount of CO released.

For AC, Figure 10 shows that the CO evolution follows a similar trend during the start of the reaction (below 825 °C),

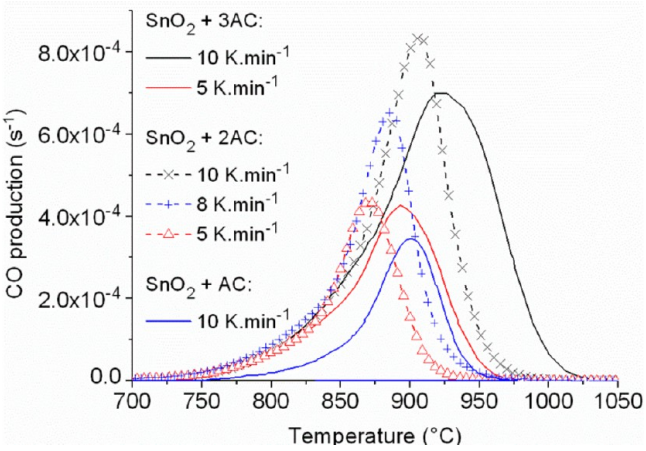

Figure 10. Instant production rate of CO as a function of the temperature using AC as the carbon source.

regardless of the operating conditions. Note that, in the particular case related to SnO_2 + AC (under stoichiometry), CO production was warped because a partial sublimation of SnO occurred (over 75% of mass loss and only melted Sn recovered), and thus, this run is not addressed in the following comments. For a given heat ramp, the CO evolution then increases faster with the lowest carbon content, which may correspond to the end of the first solid−solid reaction mechanism and the shift to the solid−gas reactions. The heating rate determines the time needed to reach the temperature region for the start of the Boudouard reaction (roughly 850 °C), so that all carbon directly in contact may be consumed especially for the lowest heating rate, thus leading to solid-state diffusion control that limits the CO production before the gas/solid reaction becomes predominant. The lower the carbon/SnO_2 ratio, the earlier and sharper the peak of CO production. With two carbons per SnO_2 in the reactant, the CO production sharpens in the range of 825−875 °C, identified as the start of the Boudouard reaction, for both heating rates. A lower carbon content is thus beneficial to hasten the rate of the reduction reaction, as stated in ref 18. Thus, the solid−solid reaction predominates when the Boudouard reaction is not favorable at low temperatures, showing similar CO production, regardless of the heating rate or carbon content. A first limitation may arise attributed to the consumption of carbon directly in contact. As the temperature rises, fewer solid−solid interactions participate, while SnO_2 reduction with CO starts. At this point, CO diffusion through the remaining carbon becomes the limiting process.

For CB, Figure 11 highlights a completely different behavior. While the CO production rates followed the same trend,

dx.doi.org/10.1021/ef402182g | Energy Fuels XXXX, XXX, XXX−XXX

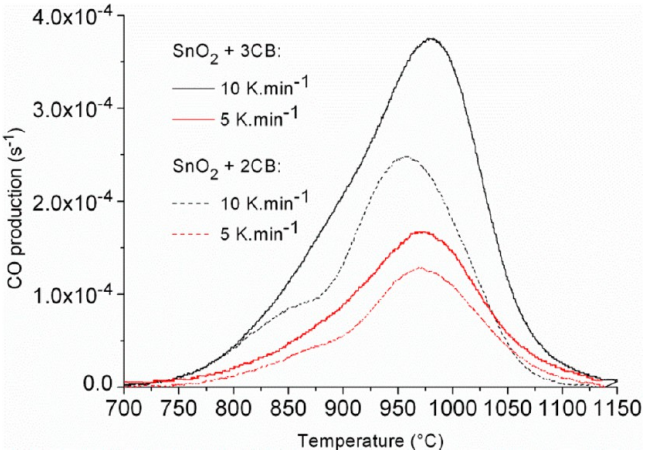

Figure 11. Instant production rate of CO as a function of the temperature using CB as the carbon source.

regardless of the conditions below 825 °C, and peaked at different temperatures for AC, the CO production rates follow different trends and have their peaks at a similar temperature (in the range of 950−1000 °C) for CB. An increase in the carbon content favors the reaction, regardless of the temperature. Inflection points are visible for both CO production curves at the lowest carbon content. Because of the nano size of the CB, the solid−solid reaction rapidly consumes the particles directly in contact, thus limiting the extent of reaction for the SnO_2 + 2CB reactant, because of solid-state diffusion limitations before the start of the Boudouard reaction.

3.2.3. Kinetic Analysis. The following general law based on Arrhenius expression is generally used to describe the kinetic rate evolution of a chemical solid-state system:

$$\frac{d\alpha}{dt} = A \exp\left(\frac{-E_a}{RT}\right) f(\alpha) \tag{8}$$

where α is the reacted fraction at time t, T is the temperature of the reactant, R is the gas constant, A is the pre-exponential factor, E_a is the activation energy, and $f(\alpha)$ is a function depending upon the reaction mechanism (see Table 4). The three latter parameters form the triplet of kinetic parameters to be determined. A classical experimental regression technique can be used to determine the value of A and E_a parameters knowing the reaction mechanism via the logarithm of eq 8.

$$\ln\left(\frac{d\alpha}{dt}\right) - \ln(f(\alpha)) = \ln(A) - \frac{1}{RT}E_a \tag{9}$$

Gotor et al.[22] have proposed a general method to determine the reaction mechanism when the activation energy is known. Taking the point of conversion 0.5 as a reference, one can write

$$\frac{f(\alpha)}{f(0.5)} = \frac{d\alpha/dt}{(d\alpha/dt)_{\alpha=0.5}} \frac{\exp(E_a/RT)}{\exp(E_a/RT_{0.5})} \tag{10}$$

Thus, by comparing the curves corresponding to various models (left part of eq 10) to experimental curves (right part of eq 10), the most seemingly adequate model can be identified.

To evaluate the reaction mechanism participating in the carbothermal reduction reaction, the master plot technique was applied to the TGA data. Accordingly, an excess of carbon (three carbons per SnO_2) compared to the reaction stoichiometry was considered to avoid inherent limitation because of the lack of reactant that may alter the kinetic results. Using the previously reported value for the activation energy of 220 kJ/mol,[18] the reaction with CB is well-represented by an unimolecular decay law that denotes a first-order surface reaction (F1 model), while the reaction with AC presents a different mechanism (Figure 12). To ascertain the value used, a

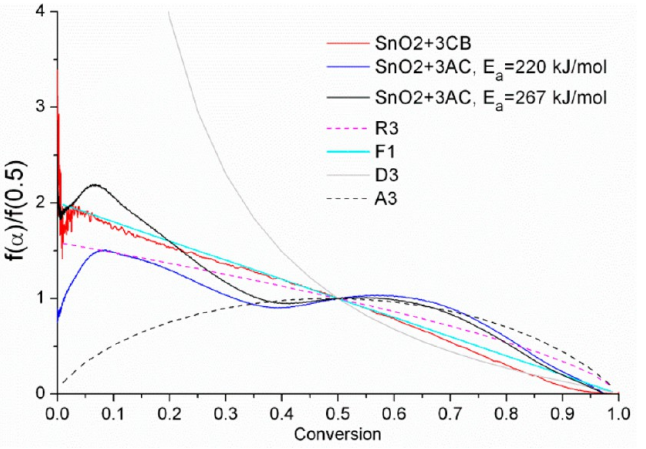

Figure 12. Master plots of various models compared to experimental results.

linear regression was performed. A smaller value of activation energy of 203.5 kJ/mol was obtained for CB (Figure 13), which does not significantly change its master plot, thus confirming both the activation energy value and mechanism. For AC, no reaction mechanism/activation energy couple provides coherent fitting, as the result of the competition between solid−solid and solid−gas reactions, coupled with gas diffusion limitations. Thus, the F1 model was also chosen for AC to describe the whole experiment. The resulting value for the activation energy

Table 4. Expression of the Reaction Mechanism $f(\alpha)$ for the Most Common Solid-State Reactions

reaction mechanism	symbol	$f(\alpha)$
phase-boundary controlled reaction (2D)	R2	$(1-\alpha)^{1/2}$
phase-boundary controlled reaction (3D)	R3	$(1-\alpha)^{2/3}$
decay law	Fn	$(1-\alpha)^{n}$
Random nucleation and growth of nuclei (Jonhson−Mehl−Avrami)	Am	$m(1-\alpha)[-\ln(1-\alpha)]^{1-1/m}$
2D diffusion	D2	$1/[-\ln(1-\alpha)]$
3D diffusion (Jander)	D3	$\frac{3(1-\alpha)^{2/3}}{2[1-(1-\alpha)^{1/3}]}$
3D diffusion (Ginstein−Brounshtein)	D4	$\frac{3}{2[(1-\alpha)^{-1/3}-1]}$

dx.doi.org/10.1021/ef402182g | Energy Fuels XXXX, XXX, XXX−XXX

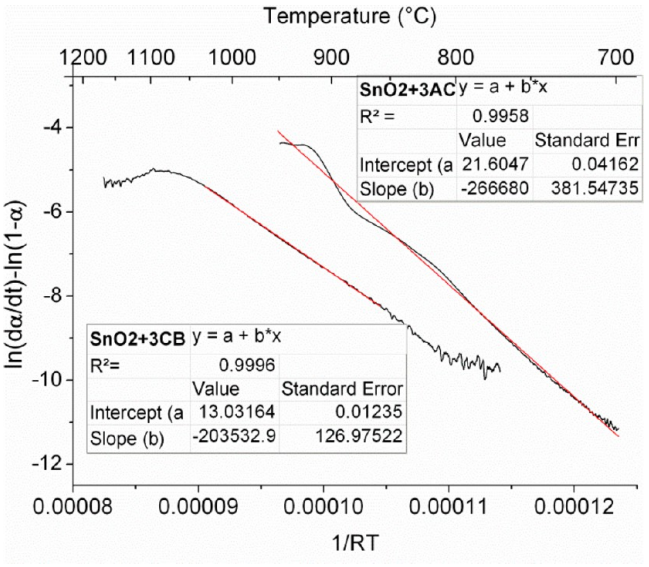

Figure 13. Linear regression analysis for SnO_2 + 3CB and SnO_2 + 3AC, with the unimolecular decay law (F1) assumed.

is 266.7 kJ/mol. The corresponding master plot logically varies around the F1 model, confirming the overall coherence of this model as an approximation.

Even though carbothermal reduction with CB starts at a higher temperature than with AC, it shows lower activation energy compared to other types of carbon (parameter values reported in Table 5) and a clearly identified first-order reaction

Table 5. Summary of Kinetic Parameters for SnO_2 Carbothermal Reduction with Different Types of Carbon

carbon type	activation energy (kJ mol^{-1})	pre-exponential factor (s^{-1})
CB	203.5 ± 0.1	$4.6 \times 10^5 \pm 5.6 \times 10^3$
	R^2 = 0.9996	
AC (apparent value)	266.7 ± 0.4	$2.4 \times 10^9 \pm 1 \times 10^8$
	R^2 = 0.9958	
coconut charcoal[18]	220.9	
graphite[18]	323.8	
beech charcoal[17]	235.4	

mechanism. Results thus provided evidence of distinct reaction paths for SnO_2 carbothermal reduction depending upon the type of carbon.

3.2.4. Carbon Gasification in the Presence of CO_2. To provide evidence of the different reaction mechanisms taking part in reaction systems, AC and CB gasification in the presence of CO_2 was conducted in a TGA (20% CO_2 in Ar flow) with various isothermal steps (Figure 14). Figure 15 compares the rate of mass loss relative to the initial mass remaining at the start of each isothermal stage. The gasification of AC and CB follows a similar rate in the range of 900−950 °C, although the reaction with AC starts at a lower temperature (800 °C). As the temperature rises, the reaction rate for CB follows a steeper trend than for AC, which tends to level off from 1020 °C because the kinetic rate is much faster than the mass-transfer rate and the reaction rate becomes controlled by external mass transfer in the gas phase at high temperature (diffusion limitations). A linear regression leads to activation energies of 178 and 194 kJ mol^{-1} for CB and AC gasification with CO_2, respectively (assuming a zero-order reaction).

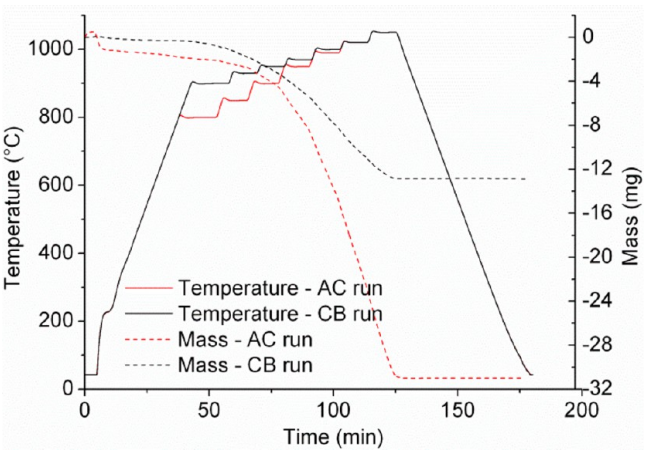

Figure 14. TGA for AC and CB gasification with 20% CO_2 in Ar flow.

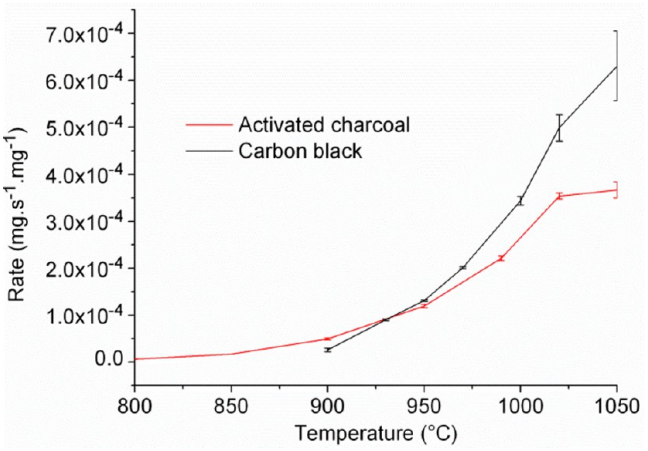

Figure 15. Experimental reaction rate of AC and CB gasification with 20% CO_2 in Ar flow.

If the Boudouard reaction was the rate-controlling step during carbothermal reduction of SnO_2 (as reported in refs 17 and 18), the reaction rate for AC and CB would be similar below 950 °C and carbothermal reduction with CB would be faster from 950 °C, which is not the case. Therefore, this confirms that the two-step gas−solid mechanism is not sufficient to explain the experimental results. A predominance of solid−solid reactions is observed for CB, whereas a predominance of solid−gas reactions is observed for AC.

3.3. Influence of the Experimental Parameters on CO_2/CO Production. A high CO content in the produced gas is desirable, both to minimize the remaining unreacted carbon and to enhance the off-gas energy content. Figure 16 summarizes the CO_2/CO overall ratios obtained in the tube flow reactor as a function of the experimental parameters. CO is much more present than reported in a previous study (from 0.95 to 2.5 mol_{CO_2}/mol_{CO} reported in ref 17). The major differences presumably come from the operating conditions, including the much smaller carbon powder size and the lower sweeping gas flow rate in the present study. These characteristics result in improved reaction surface and gas residence time that both tend to promote CO_2 conversion to CO.

A slow heating rate and carbon excess favor a high CO content in the off-gas. Reactions with AC result in the highest CO content in the off-gas, reaching the point to which no CO_2 is present for large carbon excess and low heating rate. A higher

dx.doi.org/10.1021/ef402182g | Energy Fuels XXXX, XXX, XXX−XXX

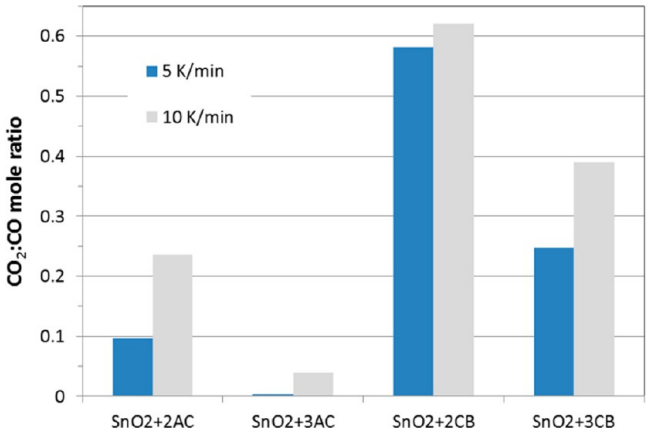

Figure 16. Influence of the experimental parameters on the CO_2/CO selectivity.

selectivity toward CO may have been expected for CB because the Boudouard reaction proceeds faster with CB (Figure 15), which denotes that solid/gas reactions are not predominant in the case of CB.

3.4. Characterization of the Products. The final products were characterized via X-ray diffraction (XRD; Panalytical X'PERT PRO diffractometer with Cu Kα radiation; αCu = 0.15406 nm; angular range = 10−100° at 2θ). As previously reported, only traces of SnO were detected. For CB-containing samples, only Sn can be detected, whereas a non-negligible amount of unreacted SnO_2 is found in the samples containing AC. The reaction thus reaches completion with CB only. Despite a better CO_2 to CO conversion and a lower starting temperature, the reaction with AC presents a lower SnO_2 final conversion that can be assigned to the diffusion limitations associated with the gas/solid reactions. An elemental balance on oxygen was also used on the basis of the comparison between the initial oxygen content in the SnO_2 reactant and the amount of oxygen contained in the gas-released species (CO and CO_2), which confirmed that residual SnO_2 was remaining in the final product for the reaction with AC. Note that, apart from the SnO_2 + AC run, in which only melted tin remained at the end of the reaction, no macroscopic modification of the powder morphology was observed because of the dispersion of SnO_2 particles in carbon, in agreement with a previous study.[17] However, the formation of finely dispersed metallic Sn droplets occurred for both AC and CB, along with coating of carbon particle agglomerates with small Sn particles (Figure 17), according to microscopy observations (using a Leica DCM3D upright microscope).

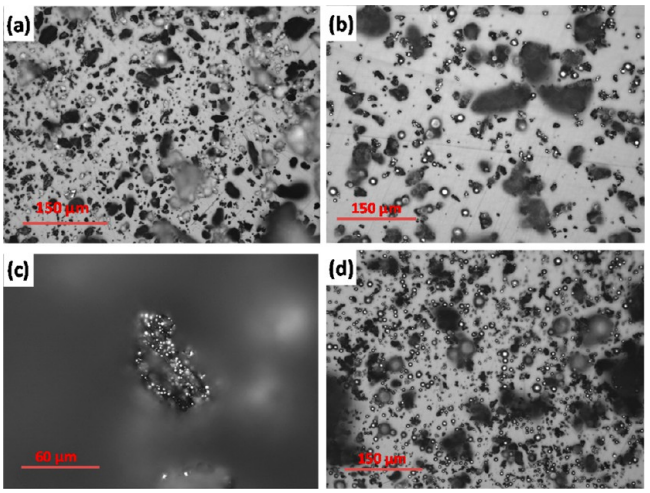

Figure 17. Microscopy observations of (a) SnO_2 + 3AC powder before reaction (SnO_2 and AC particles are clearly distinguishable), (b) SnO_2 + 3AC after reaction (dispersed metallic tin particles glint), (c) zoom of the AC particle coated with tin, and (d) SnO_2 + 3CB after reaction with the formation of dispersed metallic tin.

4. CONCLUSION

Thermodynamics shows an interesting potential for the use of CB obtained from solar methane cracking in the carbothermal SnO_2/C/Sn cycle, with an overall exergy efficiency of 86% compared to 71.6% for the most advanced carbothermal cycle, ZnO/C/Zn (both results taking into account the methane cracking). The improved efficiency for the tin-based system is mainly due to a lower reduction temperature, which decreases the re-radiation losses, and relieved requirement for quenching the gaseous products. Experimental investigation of SnO_2 carbothermal reduction was performed for different amorphous carbon sources, a high specific surface area AC and a nanosized CB obtained via solar methane cracking, to elucidate the reaction mechanisms. The reaction with AC proceeds at a lower temperature with a better CO_2 conversion into CO thanks to its high specific surface area that promotes the Boudouard solid/gas reaction. An excess of carbon is thus not desirable for AC because it creates a diffusion-limited regime (diffusion of CO through carbon). On the other hand, the activation energy is reduced with CB (204 versus 267 kJ mol^{-1}), featuring a mechanism identified as a first-order surface reaction, and a higher final chemical conversion is attained thanks to a better contact between reactants that promotes the solid−solid reactions. For CB, an excess of carbon is beneficial to counteract the consumption of carbon particles in contact with SnO_2. Despite a higher reaction temperature, a lower reaction rate, and an undesirable excess of carbon, SnO_2 carbothermal reduction with CB also presents interesting features (controllability, lower activation energy, complete SnO_2 conversion, and high CO_2 to CO conversion) compared to previously investigated carbon sources. It may become an interesting pathway toward cleaner energy, improving both carbothermal reduction processes and methane cracking profitability and proposing a possible alternative application for the solar-produced CB in complement with the other common industrial applications. Future work should concern the investigation of the use of CB as a reducing agent in solar redox cycles for fuel generation, focusing the influence of the CB characteristics on the reaction rate, and the comparison to carbothermal cycle using wood charcoal as a reducer.

AUTHOR INFORMATION

Corresponding Author

*Telephone: +33-4-68-30-77-30. Fax: +33-4-68-30-77-99. E-mail: stephane.abanades@promes.cnrs.fr.

Notes

The authors declare no competing financial interest.

ACKNOWLEDGMENTS

The financial support of the EADS foundation (CNRS CT 084210) is gratefully acknowledged. The authors also thank E. Bêche and D. Perarnau for XRD characterization.

REFERENCES

(1) Smestad, G. P.; Steinfeld, A. Review: Photochemical and thermochemical production of solar fuels from H_2O and CO_2 using metal oxide catalysts. *Ind. Eng. Chem. Res.* **2012**, *51*, 11828−11840.

(2) Graves, C.; Ebbesen, S. D.; Mogensen, M.; Lackner, K. S. Sustainable hydrocarbon fuels by recycling CO_2 and H_2O with renewable or nuclear energy. *Renewable Sustainable Energy Rev.* **2011**, *15*, 1−23.

(3) Abbas, H. F.; Wan Daud, W. M. A. Hydrogen production by methane decomposition: A review. *Int. J. Hydrogen Energy* **2010**, *35*, 1160−1190.

(4) Rodat, S.; Abanades, S.; Sans, J.-L.; Flamant, G. Hydrogen production from solar thermal dissociation of natural gas: development of a 10 kW solar chemical reactor prototype. *Sol. Energy* **2009**, *83*, 1599−1610.

(5) Abanades, S. CO_2 and H_2O reduction by solar thermochemical looping using SnO_2/SnO redox reactions: Thermogravimetric analysis. *Int. J. Hydrogen Energy* **2012**, *37*, 8223−8231.

(6) Rodat, S.; Abanades, S.; Flamant, G. Co-production of hydrogen and carbon black from solar thermal methane splitting in a tubular reactor prototype. *Sol. Energy* **2011**, *85*, 645−652.

(7) Rodat, S.; Abanades, S.; Sans, J.-L.; Flamant, G. A pilot-scale solar reactor for the production of hydrogen and carbon black from methane splitting. *Int. J. Hydrogen Energy* **2010**, *35*, 7748−7758.

(8) Rodat, S.; Abanades, S.; Flamant, G. High-temperature solar methane dissociation in a multitubular cavity-type reactor in the temperature range 1823−2073 K. *Energy Fuels* **2009**, *23*, 2666−2674.

(9) Rodat, S.; Abanades, S.; Grivei, E.; Patrianakos, G.; Zygogianni, A.; Konstandopoulos, A. G.; Flamant, G. Characterisation of carbon blacks produced by solar thermal dissociation of methane. *Carbon* **2011**, *49*, 3084−3091.

(10) Funk, J. E.; Reinstrom, R. M. Energy requirements in production of hydrogen from water. *Ind. Eng. Chem. Process Des. Dev.* **1966**, *5*, 336−342.

(11) Abraham, B. M.; Schreiner, F. General principles underlying chemical cycles which thermally decompose water into the elements. *Ind. Eng. Chem. Fundam.* **1974**, *13*, 305−310.

(12) Abanades, S.; Charvin, P.; Flamant, G.; Neveu, P. Screening of water-splitting thermochemical cycles potentially attractive for hydrogen production by concentrated solar energy. *Energy* **2006**, *31*, 2805−2822.

(13) Gálvez, M. E.; Frei, A.; Meier, F.; Steinfeld, A. Production of AlN by carbothermal and methanothermal reduction of Al_2O_3 in a N_2 flow using concentrated thermal radiation. *Ind. Eng. Chem. Res.* **2009**, *48*, 528−533.

(14) Hirsch, D.; Epstein, M.; Steinfeld, A. The solar thermal decarbonization of natural gas. *Int. J. Hydrogen Energy* **2001**, *26*, 1023−1033.

(15) Wieckert, C.; Frommherz, U.; Kräupl, S.; Guillot, E.; Olalde, G.; Epstein, M.; Santén, S.; Osinga, T.; Steinfeld, A. A 300 kW solar chemical pilot plant for the carbothermic production of zinc. *J. Sol. Energy Eng.* **2007**, *129*, 190.

(16) Osinga, T.; Olalde, G.; Steinfeld, A. Solar carbothermal reduction of ZnO: Shrinking packed-bed reactor modeling and experimental validation. *Ind. Eng. Chem. Res.* **2004**, *43*, 7981−7988.

(17) Epstein, M.; Vishnevetsky, I.; Berman, A. The SnO_2/Sn carbothermic cycle for splitting water and production of hydrogen. *J. Sol. Energy Eng.* **2010**, *132*, 031007.

(18) Padilla, R.; Sohn, H. Y. The reduction of stannic oxide with carbon. *Metall. Trans. B* **1979**, *10*, 109−115.

(19) Forster, M. Theoretical investigation of the system SnO_x/Sn for the thermochemical storage of solar energy. *Energy* **2004**, *29*, 789−799.

(20) Vishnevetsky, I.; Epstein, M. Tin as a possible candidate for solar thermochemical redox process for hydrogen production. *J. Sol. Energy Eng.* **2009**, *131*, 021007.

(21) Roine, A. *Outokumpu HSC Chemistry for Windows*; Outokumpu Research Oy: Finland, 2002.

(22) Gotor, F. J.; Criado, J. M.; Malek, J.; Koga, N. Kinetic analysis of solid-state reactions: The universality of master plots for analyzing isothermal and nonisothermal experiments. *J. Phys. Chem. A* **2000**, *104*, 10777−10782.